THE JOURNAL OF PHYSICAL CHEMISTRY C

Article

pubs.acs.org/JPCC

Colloidal Arenethiolate-Capped PbS Quantum Dots: Optoelectronic Properties, Self-Assembly, and Application in Solution-Cast Photovoltaics

Carlo Giansante,*[,†,‡] Luigi Carbone,[§] Cinzia Giannini,[∥] Davide Altamura,[∥] Zoobia Ameer,[⊥] Giuseppe Maruccio,[†,‡,⊥] Anna Loiudice,[†] Maria R. Belviso,[‡] P. Davide Cozzoli,[‡,⊥] Aurora Rizzo,[†,‡] and Giuseppe Gigli[†,‡,⊥]

[†]Center for Biomolecular Nanotechnologies @UNILE, Istituto Italiano di Tecnologia, via Barsanti 1, 73010 Arnesano (LE), Italy

[‡]NNL-CNR Istituto di Nanoscienze, via per Arnesano, 73100 Lecce, Italy

[§]IPCF-CNR UOS di Pisa, Via G. Moruzzi 1, 56124 Pisa, Italy

[∥]IC−CNR Istituto di Crystallografia, via Amendola 122/O, 70126 Bari, Italy

[⊥]Dipartimento di Matematica e Fisica 'E. De Giorgi', Università del Salento, via per Arnesano, 73100 Lecce, Italy

Supporting Information

ABSTRACT: Suitable postsynthesis surface modification of lead-chalcogenide quantum dots (QDs) is crucial to enable their integration in photovoltaic devices. Here we exploit arenethiolate anions to completely replace pristine oleate ligands on PbS QDs in the solution phase, thus preserving the colloidal stability of QDs and allowing their solution-based processability into photoconductive thin films. Complete QD surface modification relies on the stronger acidic character of arenethiols compared to that of alkanethiols and is demonstrated by FTIR and UV−vis−NIR absorption spectroscopy analyses, which provide quantitative evaluation of stoichiometry and thermodynamic stability of the resulting system. Arenethiolate ligands induce a noticeable reduction of the optical band gap of PbS QDs, which is described and explained by charge transfer interactions occurring at the organic/inorganic interface that relax exciton confinement, and a large increase of QD molar absorption coefficient, achieved through the conjugated moiety of the replacing ligands. In addition, surface modification in the solution phase promotes switching of the symmetry of PbS QD self-assembled superlattices from hexagonal to cubic close packing, which is accompanied by further reduction of the optical band gap, ascribed to inter-QD exciton delocalization and dielectric effects, together with a drastic improvement of the charge transport properties in PbS QD solids. As a result, smooth dense-packed thin films of arenethiolate-capped PbS QDs can be integrated in heterojunction solar cells via a single solution-processing step. Such single PbS QD layers exhibit abated cracking upon thermal or chemical postdeposition treatment, and the corresponding devices generate remarkable photocurrent densities and overall efficiencies, thus representing an effective strategy toward low-cost processing for QD-based photovoltaics.

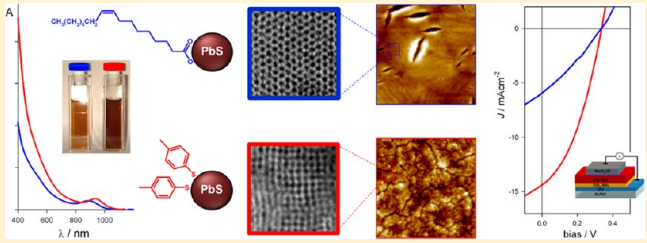

1. INTRODUCTION

Colloidal lead-chalcogenide quantum dots (QDs) have emerged as a promising class of semiconducting materials for photovoltaic applications due to the overlap of their absorption spectrum with the solar radiation,[1] large molar absorption coefficients, and small effective masses of charge carriers,[2] together with their compatibility with cost-effective solution processing.[3] The possibility of multiple exciton generation[4] and hot-carrier extraction[5] offers the opportunity to further improve the photon-to-charge-carrier conversion efficiencies by reducing losses of high-energy carriers.

Size control of semiconducting QDs permits tuning of band-edge energies thanks to the quantum confinement effect: indeed, lead sulfide QDs are particularly attractive as the active layer in heterojunction solar cells when their diameter is about 3 nm, which allows simultaneous maximization of solar light harvesting, photoinduced electron transfer rate to suitable transition metal oxides, built-in potential, and stability in air.[6,7] However, small QDs are characterized by large surface-to-volume ratio. As a consequence, the optoelectronic properties of wet-chemically synthesized lead-chalcogenide QDs are strongly dependent on their surface chemistry,[8] which is mainly dictated by the nature and bonding mode of the capping ligands. Moreover, surface-bound ligands markedly influence the interactions of QDs with the surroundings, thus affecting their propensity to closely pack into ordered assemblies,[9,10]

Received: March 28, 2013
Revised: May 13, 2013
Published: May 28, 2013

Scheme 1. Scheme of the Solution-Phase Surface Modification Strategy Employed to Replace Ol^- Molecules with ArS^- Molecules on PbS QDs Using the $ArS^-/TEA{\cdot}H^+$ Ionic Couple[a]

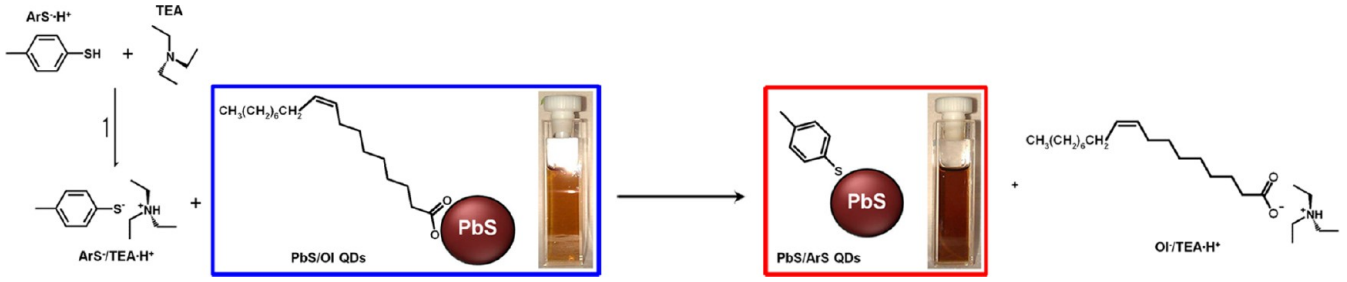

[a]Daylight pictures of 5 μM air-equilibrated dichloromethane solutions of 2.8 nm diameter PbS/Ol QDs and PbS/ArS QDs show good colloidal stability.

with dimensions up to the size scale required for useful optoelectronic applications.

In most cases, organic ligands are already introduced during the synthetic procedure, whereby they play a key role in controlling nucleation and growth of lead-chalcogenide QDs[11] and guarantee their solubility and subsequent solution processability for the fabrication of thin-film devices thereof. These pristine ligands are generally electrically insulating aliphatic long-chain compounds that have a deleterious effect on conductivity and carrier mobility in films due to inter-QD insulation, thus limiting the usefulness of colloidal QDs in optoelectronic devices. The replacement of pristine ligands has proven to be crucial in conferring appreciable conductivity to QD-based thin films.[12] Indeed, two main approaches have been employed to enhance inter-QD coupling:[3,13] (i) solid-phase ligand exchange, which entails first assembling the QDs into thin films, followed by treatment with a solution containing the replacing ligands and (ii) solution-phase ligand exchange, which involves replacing the pristine ligands on QDs that are free-standing in a liquid medium with shorter ligands capable of preserving QD solubility. The latter approach is particularly attractive as it enables the formation of smooth dense-packed solids with short inter-QD separation through few processing steps. Furthermore, the surface of QDs free-standing in solution is completely accessible to the replacing ligands, thus ensuring better passivation of recombination centers. In contrast, solid-phase ligand exchange frequently induces the formation of cracks within QD thin films due to the volume contraction resulting from bulky ligand replacement, and consequently, a tedious layer-by-layer approach is required to backfill voids. Despite such drawbacks, chemical surface modification of lead-chalcogenide QDs has been extensively performed using the solid-phase approach in view of their stronger propensity to oxidation,[14] coalescence,[15] and aggregation when the solution-phase approach is employed. On the basis of the fact that inter-QD coupling depends exponentially on interparticle distance, solid-phase ligand exchange is being performed, employing increasingly shorter ligands. To this aim, small molecules bearing amines,[12,16] thiols,[6,17−19] and carboxylic moieties[20,21] as anchoring groups and inorganic ligands based on thiocyanate[22,23] and tetrafluoroborate[24,25] salts have been widely used. Currently, atomic replacing ligands such as halide[26] or chalcogenide[27,28] anions are being extensively explored. This strategy has led to improve the mobility in QD-based solids and consequently the photovoltaic performances of corresponding devices, although it has been argued that merely pursuing large carrier mobility may not be sufficient to improve light power conversion efficiencies.[29] On the other hand, solution-phase ligand exchange has been rarely applied to lead-chalcogenide QDs because the most commonly exploited replacing ligands such as halide salts,[30,31] alkylamines,[14] dithiocarbamate derivatives,[32] or ethanethiol[15] inefficiently substitute the pristine ligands and/or frequently induce QD etching or coalescence. More effective solution-phase ligand exchange procedures require use of water[33,34] or of hazardous chemicals such as in the case of metal−chalcogenide complexes,[35] which however could be deleterious for photovoltaic device integration.

Here we exploit the stronger acidic character of arenethiols compared to that of alkanethiols to produce strongly nucleophilic thiolate-terminating ligands, which completely replace the pristine oleate ligands on the surface of PbS QDs in the solution phase (Scheme 1). We thus obtain arenethiolate-capped PbS QDs (henceforth referred to as PbS/ArS QDs) with good long-term colloidal stability, which allows solution-based deposition of PbS QDs into smooth dense-packed photoconductive thin films. Chemical surface modification markedly affects intra- and inter-QD optoelectronic and supra-QD interactions: indeed, arenethiolate ligands induce (i) a reduction of the optical band gap of PbS colloidal QDs, attributed to charge transfer interactions at the organic/inorganic interface from the sulfur anchoring atom of the replacing ligands to the PbS core, that relax exciton confinement; (ii) a large increase of the molar absorption coefficient of colloidal PbS QDs, achieved through the conjugated moiety of the replacing ligands; (iii) a switching of the symmetry of PbS QD self-assembled superlattices from hexagonal to cubic close-packing accompanied by shorter particle-to-particle distance, which leads to (iv) improved charge transport properties in PbS QD solids. As a result, a layer of PbS/ArS QDs, obtained via a single solution-based deposition step, can be used as the active layer in heterojunction solar cells employing colloidal anatase-TiO_2 nanorods (NRs). Such layers exhibit abated cracking upon thermal or chemical postdeposition treatment, and the corresponding devices photogenerate outstanding short-circuit current densities and remarkable power conversion efficiencies, thus providing an effective strategy toward low-cost processing for colloidal QD-based photovoltaics.

2. EXPERIMENTAL SECTION

Materials. All chemicals were of the highest purity available unless otherwise noted and were used as received. Lead Oxide (99.999%), oleic acid ($Ol^-{\cdot}H^+$, technical grade 90%), 1-

dx.doi.org/10.1021/jp403066q | J. Phys. Chem. C 2013, 117, 13305−13317

octadecene (technical grade 90%), bis(trimethylsilyl)sulfide (synthesis grade), titaniumtetraisopropoxide (99.999%), trimethylamino-*N*-oxide dihydrate (98%), 4-methylbenzenethiol ($ArS^-{\cdot}H^+$, 98%), benzenethiol (≥98%), 1-butanethiol (AlSH, 99%), and 3-mercaptoproprionic acid (MPA, ≥99%) were purchased from Sigma-Aldrich. Tri-*n*-octylphosphine (97%) was purchased from Strem Chemicals. Triethylamine (TEA, ≥99.5%) was purchased from Fluka. All solvents were anhydrous and were used as received. Acetone (99.8%) was purchased from Merck. Acetonitrile (99.8%), chloroform (99.8%), dichloromethane (DCM, 99.8%), *o*-dichlorobenzene (DCB, 99%), hexane (95%), methanol (99.8%), tetrachloroethylene (99%), and toluene (99.8%) were purchased from Sigma-Aldrich.

Nanocrystal Synthesis. Colloidal oleate-capped PbS QDs (henceforth referred to as PbS/Ol QDs) have been synthesized through a slightly modified well-established procedure.[1] Colloidal anatase-TiO_2 NRs have been obtained by a previously reported method.[36]

Solution-Phase Ligand Exchange Procedure. Colloidal PbS/ArS QDs have been obtained by adding a slight excess of $ArS^-/TEA{\cdot}H^+$ to PbS/Ol QDs, compared to that calculated by spectrophotometric titration, to a 1 mM solution at room temperature in an oxygen-free atmosphere. The amount of $ArS^-/TEA{\cdot}H^+$ has been determined adding $ArS^-{\cdot}H^+$ to almost 10 μM PbS/Ol QDs DCM solution in the presence of TEA. The bathochromic shift of the excitonic peak and the absorbance increase at 400 nm induced by ArS are used to determine the number of ArS^- equivalents giving complete solution-phase ligand exchange (Figure 2). In a typical procedure, 300 equiv of $ArS^-/TEA{\cdot}H^+$ has been added to a 1 mM PbS/Ol QDs DCM/DCB 1:1 solution. The mixture has been precipitated with hexane and methanol, centrifuged, and redispersed in DCM or DCB. Further purification steps deal with reprecipitation with hexane, centrifugation, and redispersion in DCM or DCB. Final dispersion has been thus centrifuged and passed through a 0.2 μm PTFE membrane to discard insoluble products and eventual agglomerates. The yield of the solution-phasae ligand exchange process, estimated from ICP-AES measurements, is up to 90%.

Characterization Techniques. Grazing incidence small-angle X-ray scattering (GISAXS) patterns have been acquired at the XMI-LAB.[37] Current−Voltage (i−V) characteristics have been measured on transmission line method (TLM) patterns consisting of micrometric Au junctions into a vacuum probe station. UV−vis−NIR absorption spectroscopy, fourier transform infrared spectroscopy (FTIR), transmission electron microscopy (TEM), scanning electron microscopy (SEM), atomic force microscopy (AFM), inductively coupled plasma atomic emission spectroscopy (ICP-AES), and X-ray diffraction (XRD) have been also employed to characterize PbS QDs in solution and solid phases. Technical details are given in the Supporting Information.

Photovoltaic Device Fabrication. A layer as thick as ∼100 nm of TiO_2 NRs has been deposited on a transparent conductive ITO glass under ambient conditions as already reported.[36] Subsequently, 1 mM solutions of PbS QDs in DCB/DCM 3:2 have been used to deposit by spin-coating a single layer as thick as ∼150 nm of either PbS/ArS or PbS/Ol QDs onto the TiO_2 NR thin film. A 10 nm thick layer of MoO_3 and, subsequently, an Al electrode (∼100 nm of thickness) have been thermally evaporated on the PbS QD layer. The active area of the device has been accurately determined by an optical microscope. Current density−voltage (J−V) measurements have been performed with an Air Mass 1.5 Global (AM 1.5 G) solar simulator with an irradiation intensity of 100 mW cm^{-2}. A calibrated filtered Si diode (Newport, 91150 V) has served as the reference cell for J−V measurements. All the fabrication and characterization processes have been carried out in a nitrogen-filled glovebox. Further details are given in the Supporting Information.

3. RESULTS AND DISCUSSION

3.1. Surface Modification of Colloidal PbS QDs. Colloidal PbS/Ol QDs with diameter of about 3 nm have been synthesized using lead(II)-oleate and bis(trimethylsilyl)-sulfide at a Pb^{2+} to S^{2-} precursor molar ratio of 2:1.[1] According to previous reports, PbS QDs have been determined to show a Pb-rich surface coordinated by oleate ligands.[38] Despite some criticism,[39] the notion of hard and soft acids and bases has been frequently used to discuss the stability of ligand coordination to metal cations on the QD surface.[35] On this basis, the soft character of thiolate bases is expected to lead to more stable coordination interactions with large, highly polarizable Pb cations compared to carboxylates, commonly considered as hard bases. Thiolate ligands have been thus obtained from arenethiol molecules by exploiting their stronger acidic character compared to that of alkanethiols. Indeed, *p*-methylbenzenethiol ($ArS^-{\cdot}H^+$ in Scheme 1) has been deprotonated with an equimolar amount of triethylamine (TEA in Scheme 1): according to their pK_a in water (6.5 and 10.8 for $ArS^-{\cdot}H^+$[40] and $TEA{\cdot}H^+$,[41] respectively), the equilibrium, though established in much less polar dichloromethane (DCM), shifts toward the formation of the ammonium thiolate ionic couple ($ArS^-/TEA{\cdot}H^+$ in Scheme 1).

Addition of $ArS^-/TEA{\cdot}H^+$ to PbS/Ol QDs induces the displacement of pristine oleate ligands, most likely in the form of $Ol^-/TEA{\cdot}H^+$ ionic couple (see Scheme 1); indeed, FTIR spectra show the appearance of the stretching vibration of carboxylate moieties (around 1700 cm^{-1}, Figure 1) of uncoordinated oleate molecules. Complete solution-phase QD surface modification has been achieved upon adding $ArS^-/TEA{\cdot}H^+$ to a 1 mM PbS/Ol QD solution (see

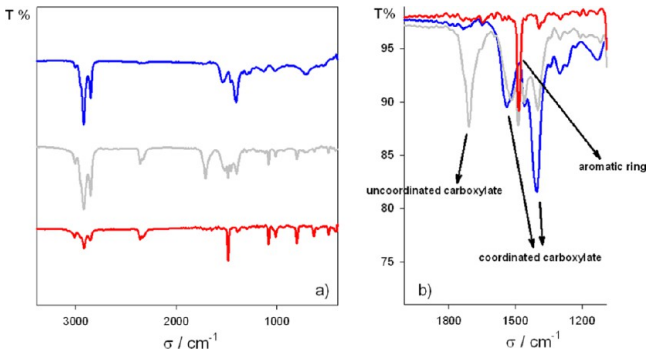

Figure 1. (a,b) FTIR spectra of thin films of PbS/Ol QDs (blue line), PbS/Ol QDs upon addition of $ArS^-/TEA{\cdot}H^+$ (gray line), and purified PbS/ArS QDs (red line). (b) Details of the FTIR spectra showing the stretching peaks at 1400 and 1540 cm^{-1} of QD-coordinated carboxylate moieties in PbS/Ol QDs (blue line), at 1700 cm^{-1} of uncoordinated carboxylate moieties upon $ArS^-/TEA{\cdot}H^+$ addition (gray line), and at 1490 cm^{-1} of the aromatic ring in purified PbS/ArS QDs (red line). The features around 2350 cm^{-1} correspond to the asymmetric stretching of carbon dioxide in air.

dx.doi.org/10.1021/jp403066q | J. Phys. Chem. C 2013, 117, 13305−13317

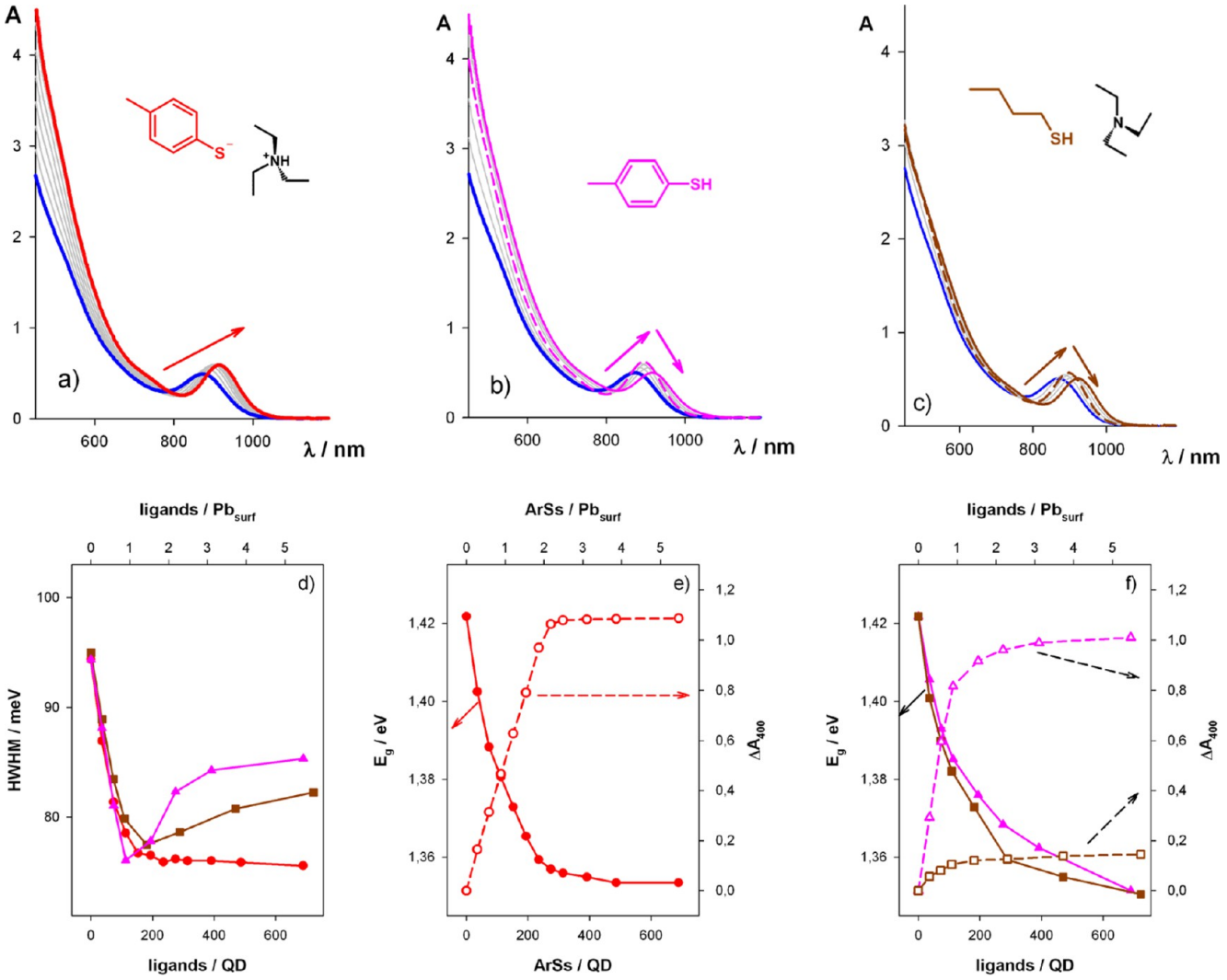

Figure 2. (a,b,c) Optical absorption spectra of 9.8 μM air-equilibrated DCM solution of PbS/Ol QDs (blue spectrum) upon addition of (a) ArS^-/$TEA{\cdot}H^+$ (red spectrum), (b) $ArS^-{\cdot}H^+$ (pink spectrum), and (c) AlSH/TEA (brown spectrum) up to 700 equiv. (d) Plot of the narrowing of the first excitonic peak of PbS QDs upon titration with ArS^-/$TEA{\cdot}H^+$ (red circles), $ArS^-{\cdot}H^+$ (pink triangles), and AlSH/TEA (brown squares). (e) Plots of the reduction of the optical band gap (full red circles) and the absorbance increase at 400 nm (empty red circles) upon addition of ArS^-/$TEA{\cdot}H^+$ to a 1.8 mM solution of PbS/Ol QDs in DCM, showing that spectral changes reach a plateau when two ArS^- ligands per excess Pb atom on the QD surface are added.[38,42] (f) plots of the reduction of the optical band gap (full symbols) and the absorbance increase at 400 nm (empty symbols) upon addition of $ArS^-{\cdot}H^+$ (pink triangles) and AlSH/TEA (brown squares) to a 1.8 mM solution of PbS/Ol QDs in DCM.

Experimental Section and Supporting Information for details). The purification steps involve quantitative precipitation with excess hexane, suggesting the efficient replacement of oleate ligands: indeed, hexane is a good solvent for PbS/Ol QDs, while it is not for PbS/ArS QDs, hence less apolar solvents have to be used to dissolve PbS/ArS QDs, such as DCM or *o*-dichlorobenzene (DCB). The yield of the solution-phase QD surface modification process, estimated from ICP-AES measurements, is up to 90%. Complete ligand exchange is demonstrated by the disappearance of carboxylate peaks in FTIR spectra and by the presence of features characteristic of ArS^- (see Figure 1). Moreover, the absence of the S−H stretching peak at around 2550−2600 cm^{-1} in the FTIR spectrum of PbS/ArS QDs suggests that the capping molecule on PbS QDs after oleate displacement is *p*-methylbenzenethiolate (ArS^-), rather than its protonated form ($ArS^-{\cdot}H^+$).

Addition of ArS^-/$TEA{\cdot}H^+$ to PbS/Ol QDs in DCM solution induces a permanent bathochromic shift and notable narrowing of the first excitonic peak, as well as a large increase in molar absorption coefficient (see Figure 2a and red symbols in panels 2d−f). Such spectral changes occur upon simple mixing of the two components (PbS QDs and ArS^- ligands) at room temperature, do not change with time, and saturate at a given ArS^- to QD molar ratio beyond which the absorption spectrum does not appreciably change, suggesting that the PbS QD surface is no longer accessible to extra added ArS^- replacing ligands. To determine whether such a saturation effect is ascribable to quantitative QD surface modification, we have estimated the number of binding sites on PbS QDs. Elemental analysis by ICP-AES revealed a Pb:S molar ratio of 1.8 for as-synthesized PbS/Ol QDs, thus allowing calculation of the number of excess Pb atoms on the QD surface,[42] under the assumption that PbS QDs consist of a stoichiometric core surrounded by an incomplete Pb shell (see Supporting Information).[38] Accordingly, spectral changes saturate upon the addition of two ArS^- ligands per excess Pb atom on the QD surface (see Figure 2e). Furthermore, the absorbance increase at 400 nm has been exploited to evaluate the thermodynamic

dx.doi.org/10.1021/jp403066q | J. Phys. Chem. C 2013, 117, 13305−13317

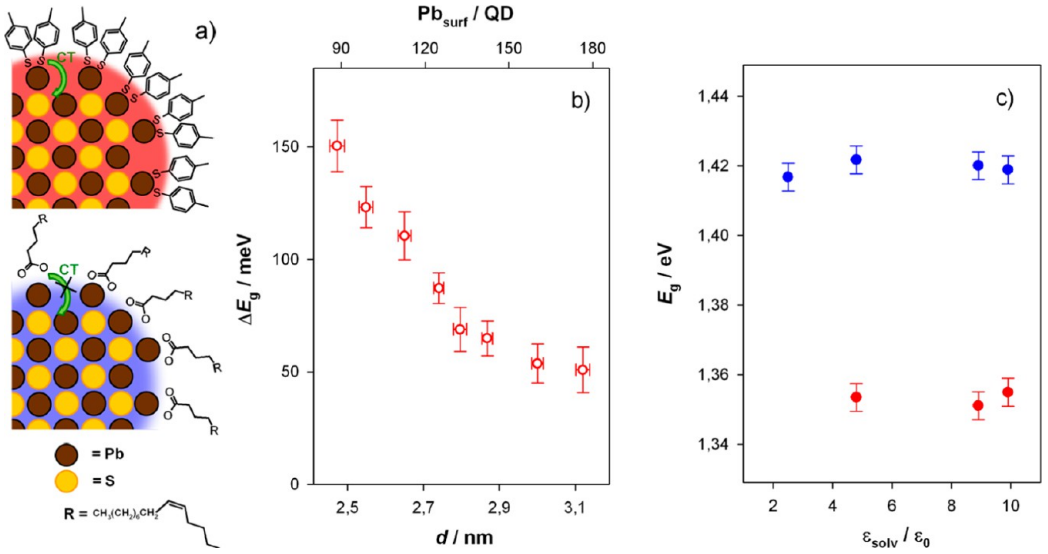

Figure 3. (a) Drawings illustrating the relaxation of exciton confinement in PbS/ArS QDs (red nuance), due to the ArS-to-QD CT interactions (green arrow); in PbS/Ol QDs, the exciton is instead confined on the inorganic core (blue nuance), resulting from the lack of interfacial CT interactions as for lead(II)−carboxylate complexes. (b) Plot of the optical band gap reduction, ΔE_g, as a function of QD diameter, d, and of the number of excess Pb atoms on the QD surface. (c) Plot of the optical band gap of PbS/Ol QDs (blue circles) and PbS/ArS QDs (red circles) in chlorinated solvents characterized by increasing dielectric constant: tetrachloroethylene, chloroform, DCM, and DCB, respectively; PbS/ArS QDs are poorly soluble in tetrachloroethylene. Symbols and error bars represent the average value and one standard deviation, respectively, calculated from at least three measurements.

stability of the PbS/ArS system, yielding a large binding constant of 1.5×10^7 M^{-1} (see Supporting Information).[43]

To ascertain the role played by TEA in the solution-phase QD surface modification procedure, we added $ArS^-{\cdot}H^+$ to PbS/Ol QDs in DCM solution. Arenethiol ligands in the absence of TEA induce a progressive red-shift of the first excitonic peak and a nonmonotonic change of its bandwidth. Such spectral changes do not saturate at any given $ArS^-{\cdot}H^+$ per QD molar ratio (see Figure 2b and pink symbols in panels d−f), accounting for the lower reproducibility of the ligand exchange process and the reduced colloidal stability of the exchanged PbS QDs, compared to those obtained with $ArS^-/TEA{\cdot}H^+$ ligands. Further confirmation arises from the spectral changes observed upon addition of 1-butanethiol (AlSH), bearing an aliphatic chain with length comparable to the *p*-methylbenzene moiety and the same anchoring group of $ArS^-{\cdot}H^+$, to PbS/Ol QDs in DCM solution. Even in the presence of TEA the addition of AlSH leads to a progressive red-shift of the first excitonic peak and nonmonotonic change of its bandwidth (see Figure 2c and brown symbols in panels d−f), similar to those observed for $ArS^-{\cdot}H^+$.

The saturation effect observed upon employing thiolate in place of thiol ligands might be related to the strong nucleophilic character of mercaptide anions and to the fact that displacement of Ol ligands bound on the QD surface would be facilitated if oleates could be converted into oleic acid molecules.[44] The lower basic character of carboxylates (pK_a for $Ol^-{\cdot}H^+$ is below 5)[45] prevents oleate protonation by thiols, while the addition of TEA to $ArS^-{\cdot}H^+$, besides producing thiolate ligands, forms $TEA{\cdot}H^+$ countercations that may facilitate the elimination of Ol ligands as triethylammonium oleate ionic couples ($Ol^-/TEA{\cdot}H^+$ in Scheme 1). The same argument holds for aliphatic thiolates, strong bases that cannot be deprotonated by Ol or TEA (pK_a for AlSH is 11.5).[40]

These findings indicate that arenethiolate ligands quantitatively replace Ol ligands on PbS QDs, without inducing aggregation and preserving good colloidal stability, from days to months depending on QD diameter: generally, the larger the QDs the less stable is their colloidal dispersion, likely due to the proportionally less effective solubilizing properties of ArS^- ligands. In this regard, we note the role of the methyl group of ArS^- that largely increases the colloidal stability in chlorinated solvents of exchanged PbS QDs, compared to the unsubstituted ring of benzenethiol. Colloidal PbS/ArS QDs can be therefore conceived as different chemical species with peculiar features by virtue of their large thermodynamic stability and clear stoichiometry.

3.2. Ground State Photophysical Properties of Colloidal PbS QDs. Figure 2a shows remarkable spectral changes occurring upon addition of $ArS^-/TEA{\cdot}H^+$ to PbS/Ol QDs. The observed red-shift of the first excitonic peak could, in principle, be explained on the basis of an increase of the QD crystalline size. However, the expected mean size changes would be much smaller than one nanometer,[46] thus highly difficult to be experimentally verified. The addition of $ArS^-/TEA{\cdot}H^+$ (or AlSH/TEA) to Pb(II)-oleate yields a yellow product consisting of amorphous Pb-thiolates without formation of PbS, even upon heating at 110 °C, the temperature at which PbS QDs have been synthesized (see Supporting Information), in agreement with previous reports.[47] In addition, since decomposition of Pb−arenethiolate complexes has been reported to take place above 200 °C,[47] growth of the QDs is unlikely to occur in the mild experimental conditions (at room temperature) of our solution-phase ligand exchange process.

We therefore discuss and explain the ArS^--induced bathochromic shift of the first excitonic peak of PbS QDs, together with its narrowing and the noticeable increase of molar absorption coefficient across the Vis−NIR spectral range, examining the organic/inorganic interface. Here we propose to describe the thiolate/QD interface in analogy to lead(II)−thiolate complexes. Indeed, we have evaluated the interaction of arenethiolate ligands with Pb atoms on the QD surface on the

dx.doi.org/10.1021/jp403066q | J. Phys. Chem. C 2013, 117, 13305−13317

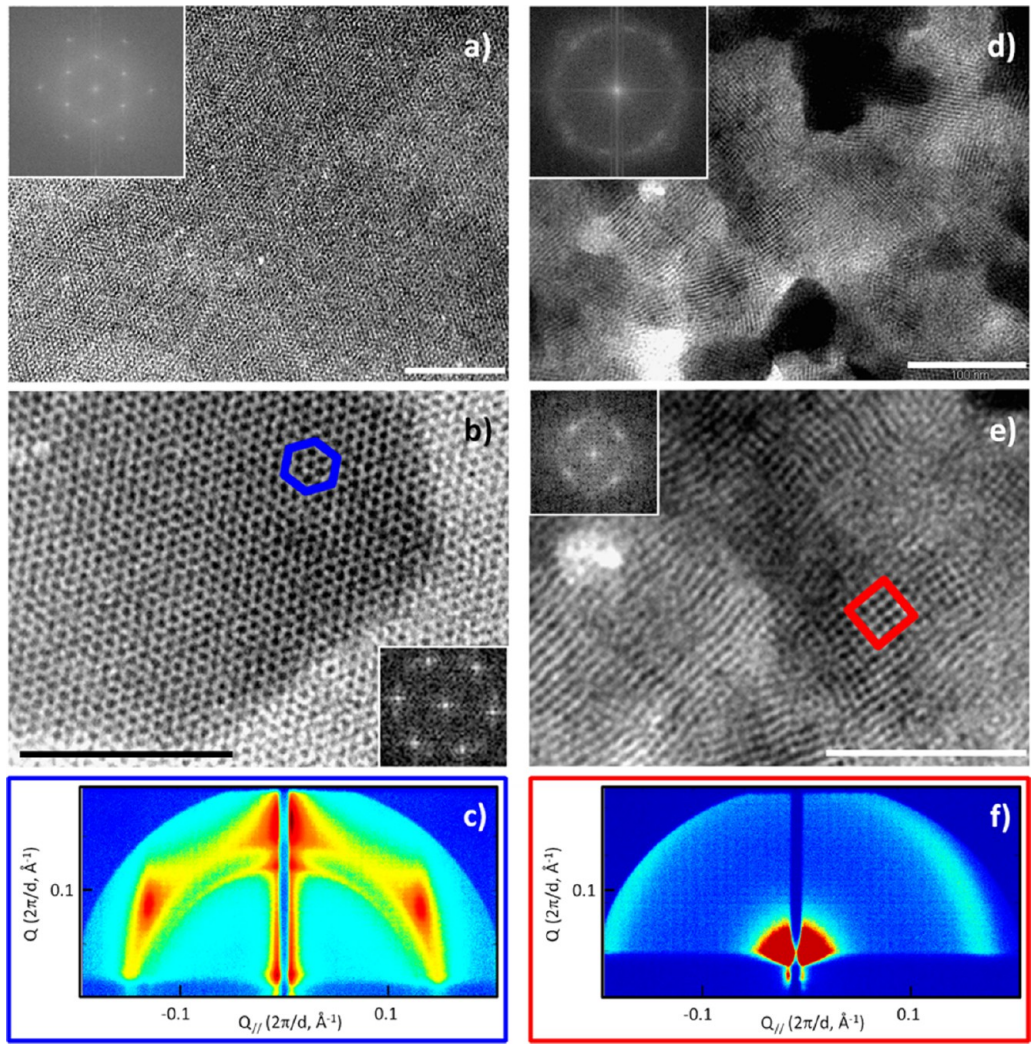

Figure 4. (a,b,d,e) TEM images at different magnification of 2.8 nm PbS QD self-assemblies capped with Ol (a,b) and ArS (d,e) molecules. Scale bar is 100 nm (a,d) or 50 nm (b,e). Polygons are drawn to emphasize the different packing motifs adopted by PbS/Ol QDs and PbS/ArS QDs. Insets show fast Fourier transform of the corresponding images. (c,f) GISAXS patterns of 2.8 nm PbS QD self-assemblies capped with Ol (c) and ArS (f) molecules.

basis of $[Pb^{II}(ArS^{-})_2]_n$ homoleptic complexes,[47,48] which show mixing of S(3p) and Pb(6p) orbitals, leading to ligand-to-metal charge transfer (CT) states.[49] We suggest that CT interactions take place at the organic/inorganic interface of PbS/ArS QDs, in analogy to those observed in lead(II)−thiolate complexes.[48,49] Such CT interactions induce delocalization of (S)3p electrons of arenethiolate ligands to the PbS QD, therefore relaxing exciton confinement and, consequently, reducing the optical band gap (Figure 3a illustrates the CT interactions at the organic/inorganic interface of colloidal PbS QDs).

The dependence of the optical band gap reduction, ΔE_g, on the QD diameter, d,[46] shown in Figure 3b is consistent with the ArS-to-QD CT mechanism: the smaller the QDs the larger the bathochromic shift, hence the larger the QD surface-to-volume ratio the larger the effect of interfacial CT processes and, consequently, the larger the extent of exciton delocalization. Considering that smaller PbS QDs within an ensemble experience a larger bathochromic shift compared to larger QDs, our model also accounts for the concomitant narrowing of the first excitonic peak of PbS QDs observed upon ArS^{-} addition (Figure 2a).

Other mechanisms already envisaged to explain the replacing ligand-induced red-shift of the first excitonic peak of colloidal QDs are not applicable to the PbS/ArS system. For instance, a mechanism based on exciton delocalization to the ligand shell, somehow related to our interfacial CT-based model, has been already proposed for PbS QDs capped with dithiocarbamate derivatives and attributed to the resonance between the top of the valence band of the PbS QDs and the HOMO of the ligands;[50] however, this model is not appropriate to our system since ArS^{-} has frontier molecular orbitals[51] energetically far from resonance with PbS QD valence and conduction band edges,[52] thus showing a potential barrier on the order of several electronvolts that hinders the energetic alignment of ArS^{-} and PbS QDs. Proceeding further, a replacing ligand-induced quantum-confined Stark effect[53] is unlikely since it requires inhomogeneous arrangements of the ArS^{-} ligands on the QD surface, not consistent with the quasi-spherical symmetry commonly assumed for PbS QDs with diameter of about 3 nm;[54] moreover, the red-shift attributed to quantum-confined Stark effect should increase for larger QDs,[55] while we observe the opposite dependence (Figure 3b). A replacing ligand-induced polarization effect, or solvatochromism,[56] can be

dx.doi.org/10.1021/jp403066q | J. Phys. Chem. C 2013, 117, 13305−13317

neglected since no appreciable shift of the first excitonic peak is observed for both PbS/Ol QDs and PbS/ArS QDs in chlorinated solvents with different polarities (blue and red circles, respectively, in Figure 3c). Such a minor polarization effect is not in contrast with the assertion of interfacial CT interactions since exciton delocalization involves prevalently the sulfur anchoring atoms as demonstrated by the extent of red-shift of the first excitonic peak observed upon addition of AlSH, or $ArS^{-}{\cdot}H^{+}$, to a PbS/Ol QD solution, similar to that observed upon addition of $ArS^{-}/TEA{\cdot}H^{+}$ (Figure 2).

The *p*-methylbenzene moiety is instead responsible for the noticeable increase in molar absorption coefficient in PbS/ArS QDs across the vis−NIR spectral range (see Figure 2 and note that $ArS^{-}/TEA{\cdot}H^{+}$ does not absorb above 300 nm). Indeed, addition of $ArS^{-}/TEA{\cdot}H^{+}$, or $ArS^{-}{\cdot}H^{+}$, to PbS/Ol QDs leads to a large absorbance increase, while the addition of AlSH is accompanied by a slight absorbance increase (Figure 2). We ascribe such a molar absorption coefficient increase to the partial mixing of (benzene)π and (S)3p orbitals[57] occurring in arenethiolate ligands. We suggest that the interaction between π electrons of the benzene ring and nonbonding electrons localized on the S anchoring atom enhances the intensity of the ArS-to-QD CT interactions. This suggestion is supported by the fact that the molar absorption coefficients reported for Pb(II)−arenethiolate complexes[48] are more than 1 order of magnitude larger than those for Pb(II)−alkanethiolate complexes.[49]

3.3. PbS QD Self-Assemblies. Besides influencing the optical properties of lead-chalcogenide QDs, the capping ligands also govern the interactions of the QDs with the surroundings, determining their solubility and also affecting their packing into ordered assemblies.[9,10]

TEM images of PbS QD self-assembled solids prepared in a vapor-saturated environment reveal a ligand-induced switching of the superlattice symmetry: by promoting self-assembly in the same experimental conditions (QD concentration, substrate, solvent, temperature, pressure, evaporation rate) PbS/Ol QDs adopt a hexagonal close-packed structure (Figure 4a,b), whereas PbS/ArS QDs exhibit a cubic close-packing motif (Figure 4d,e). PbS/ArS QD stacks lack long-range spatial coherence, showing randomly oriented domains on a submicrometer length scale.

Additional information about the average structure and inter-QD distance in the self-assemblies has been obtained by GISAXS measurements. PbS/Ol QDs self-assemble into ordered three-dimensional superlattices (leading to spot-like GISAXS patterns, as shown in Figure 4c), whereas PbS/ArS QDs show a glassy assembly (leading to ring-like GISAXS patterns, Figure 4f) likely due to the lack of long-range spatial coherence of the cubic close-packed domains already observed in TEM images.

The interaction between semiconducting QDs has been commonly described by a hard-sphere potential,[58] although this approximation does not take into account the soft character of the ligand outer shell that can markedly affect self-assembly of small QDs. Our PbS QDs show nearly spherical shape typical of small lead-chalcogenide QDs, therefore their morphology cannot be considered as the main factor underlying the symmetry of QD superlattices, which could be instead determined by a subtle balance of molecular-level noncovalent forces.[59−61] Indeed, PbS/Ol QDs and PbS/ArS QDs can be conceived as different chemical species characterized by peculiar ligand−ligand and ligand−solvent interactions, which can promote different close-packing motifs. Azimuthally integrated GISAXS intensity profiles of the PbS QD self-assemblies show a direct correlation between the capping ligand length and inter-QD separation: the center-to-center distance (L in Figure 5a) among 2.8 nm diameter PbS QDs decreases

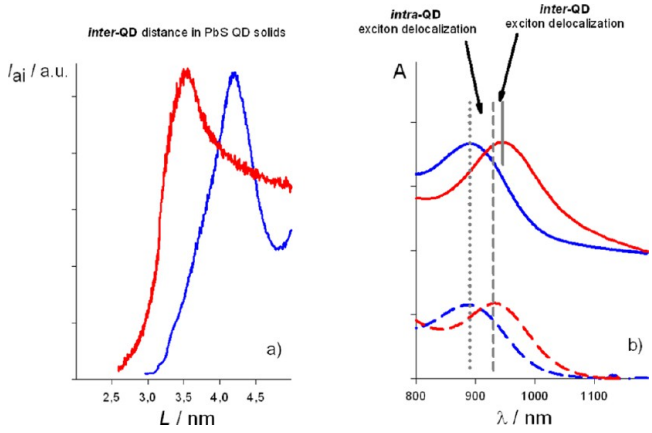

Figure 5. (a) Azimuthally integrated GISAXS intensity (I_{ai}) profiles of 2.8 nm PbS QD self-assemblies capped with Ol (blue line) and ArS (red line) molecules. (b) Optical absorption spectra of PbS QDs in DCM solution (dashed lines) and thin film (solid lines). Vertical gray lines are drawn to emphasize the shift of the first excitonic peak occurring to PbS/Ol QDs (blue spectra) and PbS/ArS QDs (red spectra). Spectra are normalized and arbitrarily vertically offset for clarity.

from 4.2 to 3.5 nm upon ligand exchange. Assuming for oleate and *p*-methylbenzenethiolate molecules lengths of around 1.8 and 0.6 nm, respectively, GISAXS measurements thus reveal the interdigitation of the capping ligands in PbS QD self-assemblies. We suggest that inter-QD hydrophobic interactions could dictate the hexagonal close-packing of PbS/Ol QD self-assembled superlattices, whereas $\pi-\pi$ interactions between arenethiolate molecules on adjacent QDs could play a relevant role in inducing the formation of the cubic close-packed domains formed by PbS/ArS QDs.

3.4. Optoelectronic Properties of PbS QD Solids. The close proximity of the PbS QDs in solid-state self-assemblies is expected to lead to mutual interactions at the ground state among QDs, which can be revealed by optical absorption measurements. PbS/Ol QDs give quite superimposable absorption spectra both in thin film and solution, whereas the absorption spectrum of the PbS/ArS QD thin film is red-shifted compared to the absorption spectrum recorded in solution (see Figure 5b). The coordination of ArS^{-} ligands to the surface of PbS QDs with diameter of 2.8 nm induces a bathochromic shift of the first excitonic peak of 70 meV, whereas PbS/ArS QD thin films are characterized by an extra red shift of about 15 meV, which is ascribable to the closer QD proximity, as determined by GISAXS measurements (Figure 5a). Indeed, contributions from electronic coupling, exciton delocalization, and dielectric effects are expected to increase with decreasing inter-QD distance. According to the Einstein−Smoluchowski relation,[18] the low field effect mobility observed in PbS/ArS QD solids (see below) accounts for negligible inter-QD electronic coupling. Therefore, both inter-QD exciton delocalization and dielectric effects are likely to be at the basis of the red-shift observed upon PbS/ArS QD thin-film formation. Consequently, the successful attainment of colloidal arenethio-

dx.doi.org/10.1021/jp403066q | J. Phys. Chem. C 2013, 117, 13305−13317

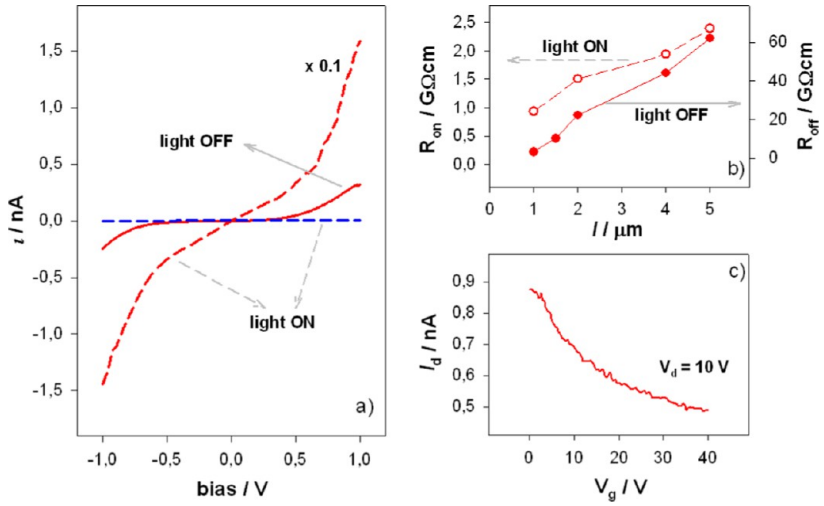

Figure 6. Current vs applied bias (i–V) characteristics of PbS/Ol QDs (blue curve) and PbS/ArS QDs (red curves) recorded at room temperature under vacuum both in the dark (solid line) and under solar-simulated illumination (dashed lines). (b) Resistance values of PbS/ArS QD thin films at different junction distances, l, both in the dark (filled circles) and under solar-simulated illumination (empty circles). (c) Drain current values at 10 V of PbS/ArS QD thin films increasing gate voltage, V_g.

late-capped PbS QDs that are free-standing in the solution phase, and self-assemblies thereof, allows us to discriminate between intra- and inter-QD interactions, whereas solid-phase ligand exchange hinders such a distinction. We therefore suggest that the red-shift observed after the postdeposition treatment of lead-chalcogenide QD solids with short thiol molecules which is commonly attributed to inter-QD electronic coupling[17−19] or to polarization effects[56] should instead be mainly ascribed to interfacial CT interactions from the (S)3p orbitals of the ArS ligands to the PbS core that relax exciton confinement at the ArS/PbS organic/inorganic interface.

To determine whether QD proximity improves charge transport in thin films, we have measured dark and photo-induced current−voltage (i–V) characteristics of PbS/Ol and PbS/ArS QDs (Figure 6). To this aim, colloidal PbS QDs have been solution-casted onto micrometric junctions consisting of gold electrodes with different separation and then rapidly transferred into a vacuum probe station, minimizing air exposure.

PbS/Ol QD thin films show rather insulating character due to the bulky oleate ligands (data not shown),[12,62] whereas a negligible current increase is observed upon solar-simulated illumination (dashed blue line in Figure 6a), as expected for systems in which the resonant energy transfer is the dominant pathway for charge transport of photogenerated electron−hole pairs.[17] On the other hand, PbS/ArS QD thin films exhibit improved charge transport properties in the dark (solid red line in Figure 6a), ascribable to their close proximity. Quantitatively, thin films of PbS/ArS QDs generate dark currents of about 300 pA at 1 V, whereas thin films of PbS/Ol QDs generate only few pA in the same experimental conditions. Using TLM patterns, PbS/ArS QD thin films show a value of resistivity, ρ, of about 10 MΩ cm, as estimated from the slope of the dependence of resistance on the distance between similar source and drain electrodes (full circles in Figure 6b). Although apparently poor, the dark charge transport properties of PbS/ArS QD thin films have to be evaluated upon considering the dependence of resistivity on QD size and inter-QD spacing, the latter being mainly determined by the ligand length. In this regard, our results are consistent with previously reports on lead-chalcogenide QD solids,[18,63−65] when the small size of PbS/ArS QDs (diameter of 2.8 nm) and their relatively large separation in thin films (around 0.7 nm, as determined by the azimuthally integrated GISAXS intensity profiles shown in Figure 5a) are taken into account. Upon solar-simulated illumination, PbS/ArS QD thin films exhibit photocurrent of about 15 nA at 1 V (dashed red curve in Figure 6a), thus showing an increase of 4 orders of magnitude compared to the current photogenerated by PbS/Ol QD thin films. Using again TLM patterns, the resistivity of PbS/ArS QD solids under solar-simulated illumination is estimated to be of about 0.2 MΩ cm (empty circles in Figure 6b). A reversible and stable switching of the photocurrent is observed upon light ON/OFF cycles as shown in the Supporting Information. Notably, the shape of the i–V curve is nonlinear, showing a less conductive central region which is compatible with the optical band gap of the PbS/ArS QDs (see Supporting Information). Despite that further dedicated investigations are necessary for the identification of the charge transport mechanism to discriminate between tunneling,[17] hopping,[62,66] or transport through intragap states,[63,67] it is however evident that the above presented solution-phase processing strategy confers noticeably photogenerated conductivity to PbS QD thin films.

The field-effect mobility, μ, has been also estimated from the transconductance on assuming an ideal FET behavior (Figure 6c),[64,65] from which a μ value of $\sim 10^{-6}$ cm^2 V^{-1} s^{-1} has been deduced. Such a μ value would correspond to a hole carrier density, p, of about 5×10^{17} cm^{-3}, if a Drude-like formula is assumed for the conductivity ($1/\rho = pe\mu$, where e stands for the elementary charge constant). The estimated hole carrier density is roughly 1 order of magnitude larger than that determined in thiol-treated PbS QD solids[6,68] and could be an indication that effective control over the balance of charges on the QD surface has been achieved by exploiting our chemical surface modification approach: indeed, ligand exchange in the solution phase ensures that the QD surface is completely accessible to replacing arenethiolate ligands, thus enabling better passivation of recombination centers than employing solid-phase ligand exchange.[69]

dx.doi.org/10.1021/jp403066q | J. Phys. Chem. C 2013, 117, 13305−13317

3.5. Photovoltaic Devices Based on PbS QDs.

The arenethiolate-induced improvement of charge transport properties in PbS QD thin films has been thus exploited in heterojunction solar cells, comprising a film of colloidal anatase-TiO_2 NRs as an electron-acceptor hole-blocking layer[36] and MoO_3 as a hole-extraction layer.[70] To this purpose, a ∼150 nm thick active layer has been obtained upon solution-casting of colloidal PbS QDs via a single deposition step, onto the TiO_2 layer (see device architecture in Figure 7; details on device fabrication procedure are given in the Experimental Section and Supporting Information).

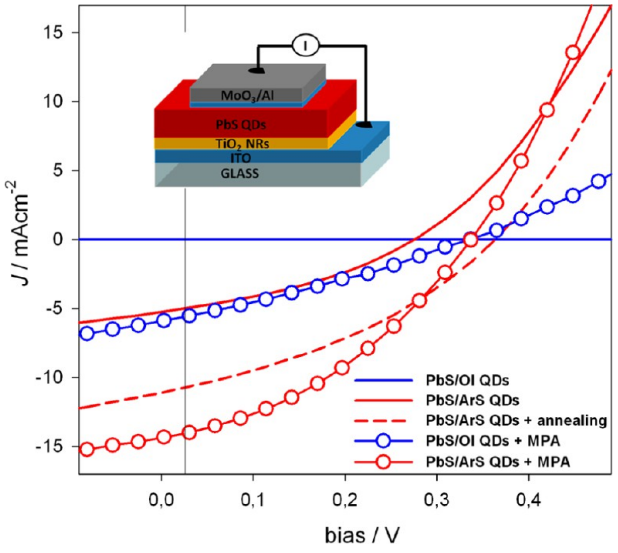

Figure 7. Current density vs applied bias ($J-V$) characteristics under 100 mW cm^{-2} simulated AM1.5 solar light illumination of the heterojunction solar cells prepared from colloidal PbS/Ol QDs (blue line), colloidal PbS/ArS QDs (solid red line), annealing at 110 °C of PbS/ArS QD solids (dashed red line), postdeposition MPA treatment of PbS/Ol QD solids (empty blue circles), and postdeposition MPA treatment of PbS/ArS QD solids (empty red circles). Inset shows a sketch of the device architecture.

The electron−hole pairs photogenerated in the light-harvesting PbS QDs are expected to separate at the heterojunction between the PbS QD electron-donor layer and the large band gap shallow work function TiO_2 NR electron-acceptor hole-blocking layer,[36,71,72] allowing the free electrons and holes to be transported to the electrodes through the anatase-TiO_2 and the PbS layers, respectively. The current density−voltage ($J-V$) characteristics of our devices under solar-simulated illumination are shown in Figure 7, and corresponding photovoltaic parameters are summarized in Table 1.

As expected, negligible photocurrent is detected in devices employing PbS/Ol QDs due to the insulating character of bulky oleate ligands that hinders charge transport among adjacent PbS QDs. As opposed, photovoltaic devices prepared from PbS/ArS QDs exhibit short-circuit photocurrent density, J_{sc}, of about 5 mA cm^{-2} under solar-simulated illumination, which corroborates previous findings on the improved charge-carrier transport properties in thin films of arenethiolate-capped PbS QDs (compare blue and red $J-V$ solid curves, respectively, in Figure 7).

Notably, our solution-phase ligand exchange approach allows depositing the photoconductive layer of PbS QDs via a single step, thus avoiding tedious layer-by-layer deposition steps, which are required when ligand exchange is carried out on the solid phase. This convenience is further demonstrated by the quality of the PbS/ArS QD active layer upon thermal or chemical postdeposition treatment.

Table 1. Photovoltaic Parameters for TiO_2 NR/PbS QD Heterojunction Solar Cells[a]

active layer	J_{sc}/mA cm^{-2}	V_{oc}/V	FF/%	η/%
PbS/Ol QDs	0.0	-	-	0.00
PbS/ArS QDs	5.16	0.28	35	0.55
PbS/ArS QDs + annealing	10.25	0.37	36	1.34
PbS/Ol QDs + MPA	5.90	0.34	29	0.58
PbS/ArS QDs + MPA	14.30	0.34	38	1.85

[a] J_{sc}, V_{oc}, FF, and η stand for short circuit current, open circuit voltage, fill factor, and power conversion efficiency, respectively.

Indeed, we mildly annealed the as-deposited PbS/ArS QD layer at 110 °C, well below the temperatures at which sintering of PbS QDs begins[73] and the *p*-methylbenzenethiol boils. The corresponding photovoltaic devices (see dashed line in Figure 7) show a remarkable increase of short-circuit photocurrent density (J_{sc} = 10.25 mA cm^{-2}) and power conversion efficiency (η = 1.34%). We therefore attribute the improved device performances to a thermal-induced reduction of the inter-QD distance that consequently improves charge transport properties of the PbS/ArS QD layer; such an attribution can be supported by the morphological characterization of the annealed PbS/ArS QD thin film (Figure 8a) which shows slightly larger voids and reduced roughness compared to the as-deposited PbS/ArS QD thin- film (see Supporting Information).

To understand whether our QD surface modification strategy is beneficial to the efficiency of the photon-to-charge-carrier conversion process, we have tested our system after applying a well-established postdeposition treatment to PbS QD solids that employ 3-mercaptopropionic acid (MPA) as the replacing ligand.[26,30] After the deposition of the single layer of either PbS/Ol QDs or PbS/ArS QDs onto the TiO_2 NR layer, few drops of MPA in acetonitrile solution have been dispensed onto the PbS QD thin films. MPA molecules have been reported to replace Ol ligands leading to smaller inter-QD separation, which ensures good photovoltaic performance of the finished devices.[6,7] Indeed, the device employing MPA-treated PbS/Ol QD solids as the active layer shows values of short-circuit photocurrent density and power conversion efficiency (J_{sc} = 5.9 mA cm^{-2} and η = 0.58%, respectively) similar to those exhibited by the device comprising the as-deposited PbS/ArS QD layer. On the other hand, such a postdeposition treatment to PbS/ArS QD solids induces, probably to a lesser extent though, the displacement of ArS ligands replaced by MPA molecules. The MPA-treated PbS/ArS QD device therefore exhibits large short-circuit photocurrent density (J_{sc} = 14.3 mA cm^{-2}) and overall efficiency, η, of 1.85%, which are remarkable for devices fabricated via a single QD deposition step.

AFM inspection of the PbS QD thin films (see Figure 8) helps us explain the differences in performance for the PbS/Ol and PbS/ArS QD-based solar cells. Albeit to different degrees, the MPA postdeposition treatment induces fissuring and buckling of the as-deposited PbS QD layers due to oleate and arenethiolate ligand replacement: indeed, upon MPA treatment, the PbS/Ol QD layers undergo extensive cracking (Figure 8b), whereas smaller cracks can be observed in the

dx.doi.org/10.1021/jp403066q | J. Phys. Chem. C 2013, 117, 13305−13317

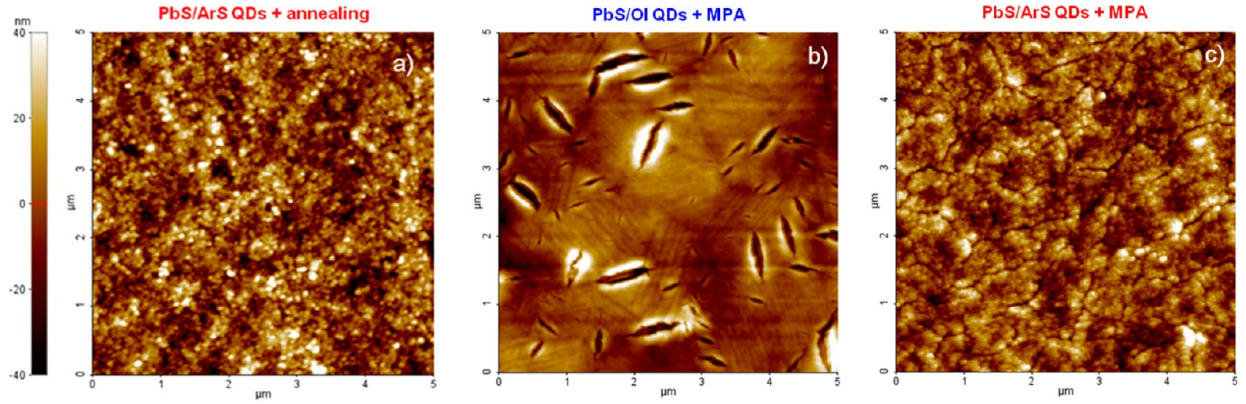

Figure 8. AFM images of annealed PbS/ArS QD layer (a), MPA-treated PbS/Ol QD layer (b), and MPA-treated PbS/ArS QD layer (c).

PbS/ArS QD layers (Figure 8c), consistent with the larger volume loss expected upon the replacement of aliphatic long chains of Ol ligands compared to short conjugated ArS molecules.

The low fill factor, compared to the conventional mesoporous TiO_2/PbS QD depleted bulk heterojunction devices, indicates significant recombination losses, which are principally attributed to traps and dangling bonds on the surface of TiO_2 NRs.[74] Moreover, the low open-circuit voltage and fill factor of our photovoltaic devices can be ascribed to the unoptimized thickness of the TiO_2 NR and PbS QD layers, when compared to conventional depleted bulk heterojunction.[6,7] Nonetheless, there is ample room to improve the device performances by enhancing the surface passivation of TiO_2 NRs and by increasing the active surface area for charge separation between PbS QD electron donors and TiO_2 NR acceptors. It is however evident that smoother morphology and improved charge-carrier transport are obtained employing PbS/ArS QDs as the active layer. Colloidal arenethiolate-capped PbS QDs may therefore represent an effective intermediate step in the fabrication of colloidal QD-based solar cells, enabling the formation of smooth dense-packed solids with short inter-QD separation through fewer processing steps, when compared to the layer-by-layer approach, which instead requires several tens of cycles of QD deposition and solid-phase ligand exchange treatment to fill the cracks.

CONCLUSIONS

The above presented postsynthesis surface modification of colloidal PbS QDs has relevant implications from both fundamental and practical points of view. Quantitative PbS QD surface modification in the solution phase is achieved by exploiting the stronger acidic character of arenethiols compared to that of alkanethiols, which produces strongly nucleophilic thiolate ligands: indeed, arenethiolates coordinate the PbS QD surface with a clear stoichiometry, of two ArS^- ligands per excess Pb atom, and a large thermodynamic stability, above 10^7 M^{-1}, therefore completely replacing the pristine insulating oleate ligands. The resulting arenethiolate-capped PbS QDs preserve good long-term colloidal stability and can be easily processed from the solution phase into smooth dense-packed photoconductive thin films via a single deposition step. Such a surface modification induces a significant bathochromic shift and narrowing of the first excitonic peak and a large absorbance increase of colloidal PbS QDs, which are explained by describing the ArS/PbS organic/inorganic interface in analogy to Pb(II)−arenethiolate complexes: we indeed suggest that interfacial CT interactions from the (S)3p orbitals of the ArS ligands to the PbS core relax exciton confinement at the ArS/PbS interface, thus leading to a reduction of the optical band gap of PbS QDs and, through the conjugated moiety of the ArS ligands, to a large increase of their molar absorption coefficient across the vis−NIR spectral range. In addition to markedly affecting optical properties of colloidal QDs, the arenethiolate shell impacts supra-QD interactions: indeed, the symmetry of PbS QD self-assembled superlattices switches from hexagonal close-packing adopted by PbS/Ol QDs to cubic close-packing observed for PbS/ArS QDs. The presence of shorter ArS ligands on the surface of PbS QDs results in tighter packing, which is accompanied by further reduction of the optical band gap, ascribed to inter-QD exciton delocalization and dielectric effects in PbS QD solids. As a result, a drastic increase of the charge transport properties in PbS/ArS QD thin films is achieved. Accordingly, we can successfully fabricate efficient heterojunction solar cells that incorporate PbS/ArS QDs as the active layer, obtained via a single solution-based deposition step on top of an electron acceptor and hole-blocking layer of TiO_2 NRs. Such single layers of PbS/ArS QDs undergo noticeably lesser cracking upon thermal and chemical postdeposition treatment, compared to PbS/Ol QD layers, and the corresponding photovoltaic cells generate short-circuit photocurrent densities and overall power conversion efficiencies, which are remarkable for devices fabricated via a single QD deposition step.

Colloidal PbS/ArS QDs can be therefore conceived as different chemical species with peculiar features by virtue of their large thermodynamic stability and clear stoichiometry. The successful attainment of arenethiolate-capped PbS QDs with good colloidal stability is crucial to discriminate between intra- and inter-QD interactions in thiol-capped lead-chalcogenide QD solids and to infer the resulting optoelectronic properties. In addition, our surface modification approach enables easy solution-phase deposition of PbS QDs into smooth dense-packed photoconductive solids in few processing steps and ensures increased control over the balance of charges on the QD surface, therefore providing further possibilities toward low-cost processing for QD-based photovoltaics.

dx.doi.org/10.1021/jp403066q | J. Phys. Chem. C 2013, 117, 13305−13317

■ ASSOCIATED CONTENT

Supporting Information

Synthesis of PbS/Ol QDs and TiO_2 NRs; solution-phase surface modification procedure for the preparation of colloidal PbS/ArS QDs; characterization techniques; photovoltaic device fabrication; PbS QD solid-state sample preparation; binding site number and stability constant calculation; TEM, SEM, and AFM images; XRD spectra; charge transport measurements. This material is available free of charge via the Internet at http://pubs.acs.org.

■ AUTHOR INFORMATION

Corresponding Author

*E-mail: carlo.giansante@iit.it.

Notes

The authors declare no competing financial interest.

■ ACKNOWLEDGMENTS

This work is dedicated to the memory of Gianluca Latini. The authors thank Rosanna Mastria, Roberto Giannuzzi, Anna Grazia Monteduro, Giovanni Lerario, Luigi Martiradonna, and Alessandra Quarta for technical support and helpful discussion. This work has been supported by the Italian projects Rete Nazionale di Ricerca sulle Nanoscienze ItalNanoNet (FIRB reference number RBPR05JH2P) and EFOR-Energia da FOnti Rinnovabili (Iniziativa CNR per il Mezzogiorno L. 191/2009 art. 2 comma 44) and by the European project ESCORT-Efficient Solar Cells based on Organic and hybrid Technology (seventh FWP - reference number 261920). This work has been partially supported by the Italian Ministry of Education, University and Research through the project AEROCOMP (contract MIUR no. DM48391) and by the SEED project "X-ray synchrotron class rotating anode microsource for the structural micro imaging of nanomaterials and engineered biotissues (XMI-LAB)"- Italian Institute of Technology (IIT) Protocol n. 21537 of 23/12/2009. Rocco Lassandro is acknowledged for the technical support with the XMI-LAB. Zoobia Ameer acknowledges the faculty development program of Pakistan Higher Education Commission (HEC) for financial support for her Ph.D.

■ REFERENCES

(1) Hines, M. A.; Scholes, G. D. Colloidal PbS Nanocrystals With Size-Tunable Near-Infrared Emission: Observation of Post-Synthesis Self-Narrowing of the Particle Size Distribution. *Adv. Mater.* **2003**, *15*, 1844−1849.

(2) Murphy, J. E.; Beard, M. C.; Norman, A. G.; Ahrenkiel, S. P.; Johnson, J. C.; Yu, P.; Mićić, O. I.; Ellingson, R. J.; Nozik, A. J. PbTe Colloidal Nanocrystals: Synthesis, Characterization, and Multiple Exciton Generation. *J. Am. Chem. Soc.* **2006**, *128*, 3241−3247.

(3) Tang, J.; Sargent, E. H. Infrared Colloidal Quantum Dots for Photovoltaics: Fundamentals and Recent Progress. *Adv. Mater.* **2011**, *23*, 12−29.4.

(4) Nozik, A. J.; Beard, M. C.; Luther, J. M.; Law, M.; Ellingson, R. J.; Johnson, J. C. Semiconductor Quantum Dots and Quantum Dot Arrays and Applications of Multiple Exciton Generation to Third-Generation Photovoltaic Solar Cells. *Chem. Rev.* **2010**, *110*, 6873−6890.

(5) Tisdale, W. A.; Williams, K. J.; Timp, B. A.; Norris, D. J.; Aydil, E. S.; Zhu, X.-Y. Hot-Electron Transfer from Semiconductor Nanocrystals. *Science* **2010**, *328*, 1543−1547.

(6) Pattantyus-Abraham, A. G.; Kramer, I. J.; Barkhouse, A. R.; Wang, X.; Konstantatos, G.; Debnath, R.; Levina, L.; Raabe, I.; Nazeeruddin, M. K.; Grätzel, M.; et al. Depleted-Heterojunction Colloidal Quantum Dot Solar Cells. *ACS Nano* **2010**, *4*, 3374−3380.

(7) Tang, J.; Brzozowski, L.; Barkhouse, D. A. R.; Wang, X.; Debnath, R.; Wolowiec, R.; Palmiano, E.; Levina, L.; Pattantyus-Abraham, A. G.; Jamakosmanovic, D.; et al. Quantum Dot Photovoltaics in the Extreme Quantum Confinement Regime: The Surface-Chemical Origins of Exceptional Air- and Light-Stability. *ACS Nano* **2010**, *4*, 869−878.

(8) Wise, F. W. Lead Salt Quantum Dots: the Limit of Strong Quantum Confinement. *Acc. Chem. Res.* **2000**, *33*, 773−780.

(9) Hanrath, T. Colloidal Nanocrystal Quantum Dot Assemblies As Artificial Solids. *J. Vac. Sci. Technol. A* **2012**, *30*, 030802.

(10) Quan, Z.; Valentin-Bromberg, L.; Loc, W. S.; Fang, J. Self-Assembly of Lead Chalcogenide Nanocrystals. *Chem. Asian J.* **2011**, *6*, 1126−1136.

(11) Cho, K.-S.; Talapin, D. V.; Gaschler, W.; Murray, C. B. Designing PbSe Nanowires and Nanorings through Oriented Attachment of Nanoparticles. *J. Am. Chem. Soc.* **2005**, *127*, 7140−7147.

(12) Talapin, D. V.; Murray, C. B. PbSe Nanocrystal Solids for n- and p-Channel Thin Film Field-Effect Transistors. *Science* **2005**, *310*, 86−89.

(13) Talapin, D. V.; Lee, J. S.; Kovalenko, M. V.; Shevchenko, E. V. Prospects of Colloidal Nanocrystals for Electronic and Optoelectronic Applications. *Chem. Rev.* **2010**, *110*, 389−458.

(14) Konstantatos, G.; Howard, I.; Fischer, A.; Hoogland, S.; Clifford, J.; Klem, E.; Levina, L.; Sargent, E. H. Ultrasensitive Solution-Cast Quantum Dot Photodetectors. *Nature* **2006**, *442*, 180−183.

(15) Hinds, S.; Levina, L.; Klem, E. J. D.; Konstantatos, G.; Sukhovatkin, V.; Sargent, E. H. Smooth-Morphology Ultrasensitive Solution-Processed Photodetectors. *Adv. Mater.* **2008**, *20*, 4398−4402.

(16) Law, M.; Luther, J. M.; Song, O.; Hughes, B. K.; Perkins, C. L.; Nozik, A. J. Structural, Optical, and Electrical Properties of PbSe Nanocrystal Solids Treated Thermally or with Simple Amines. *J. Am. Chem. Soc.* **2008**, *130*, 5974−5985.

(17) Choi, J. J.; Luria, J.; Hyun, B.-R.; Bartnik, A. C.; Sun, L.; Lim, Y.-F.; Marohn, J. A.; Wise, F. W.; Hanrath, T. Photogenerated Exciton Dissociation in Highly Coupled Lead Salt Nanocrystal Assemblies. *Nano Lett.* **2010**, *10*, 1805−1811.

(18) Liu, Y.; Gibbs, M.; Puthussery, J.; Gaik, S.; Ihly, R.; Hillhouse, H. W.; Law, M. Dependence of Carrier Mobility on Nanocrystal Size and Ligand Length in PbSe Nanocrystal Solids. *Nano Lett.* **2010**, *10*, 1960−1969.

(19) Luther, J. M.; Law, M.; Song, Q.; Perkins, C. L.; Beard, M. C.; Nozik, A. J. Structural, Optical, and Electrical Properties of Self-Assembled Films of PbSe Nanocrystals Treated with 1,2-Ethanedithiol. *ACS Nano* **2008**, *2*, 271−280.

(20) Gao, Y.; Aerts, M.; Sandeep, C. S.; Talgorn, E.; Savenije, T. J.; Kinge, S.; Siebbeles, L. D.; Houtepen, A. J. Photoconductivity of PbSe Quantum-Dot Solids: Dependence on Ligand Anchor Group and Length. *ACS Nano* **2012**, *6*, 9606−14.

(21) Zarghami, M. H.; Liu, Y.; Gibbs, M.; Gebremichael, E.; Webster, C.; Law, M. PbSe and PbS Quantum Dot Solids Prepared with Short-Chain Acids and Diacids. *ACS Nano* **2010**, *4*, 2475−2485.

(22) Koh, W.-K.; Saudari, S. R.; Fafarman, A. T.; Kagan, C. R.; Murray, C. B. Thiocyanate-Capped PbS Nanocubes: Ambipolar Transport Enables Quantum Dot Based Circuits on a Flexible Substrate. *Nano Lett.* **2011**, *11*, 4764−4767.

(23) Fafarman, A. T.; Koh, W.-K.; Diroll, B. T.; Kim, D. K.; Ko, D.-K.; Oh, S. J.; Ye, X.; Doan-Nguyen, V.; Crump, M. R.; Reifsnyder, D. C.; et al. Thiocyanate-Capped Nanocrystal Colloids: Vibrational Reporter of Surface Chemistry and Solution-Based Route to Enhanced Coupling in Nanocrystal Solids. *J. Am. Chem. Soc.* **2011**, *133*, 15753−15761.

(24) Rosen, E. L.; Buonsanti, R.; Llordes, A.; Sawvel, A. M.; Milliron, D. J.; Helms, B. A. Exceptionally Mild Reactive Stripping of Native Ligands from Nanocrystal Surfaces by Using Meerwein's Salt. *Angew. Chem., Int. Ed.* **2012**, *51*, 684−689.

(25) Dong, A.; Ye, X.; Chen, J.; Kang, Y.; Gordon, T.; Kikkawa, J. M.; Murray, C. B. A Generalized Ligand-Exchange Strategy Enabling

Sequential Surface Functionalization of Colloidal Nanocrystals. *J. Am. Chem. Soc.* **2011**, *133*, 998−1006.
(26) Tang, J.; Kemp, K. W.; Hoogland, S.; Jeong, K. S.; Liu, H.; Levina, L.; Furukawa, M.; Wang, X.; Debnath, R.; Cha, D.; et al. Colloidal-Quantum-Dot Photovoltaics Using Atomic-Ligand Passivation. *Nat. Mater.* **2011**, *10*, 765−771.
(27) Nag, A.; Kovalenko, M. V.; Lee, J.-S.; Liu, W.; Spokoyny, B.; Talapin, D. V. Metal-Free Inorganic Ligands for Colloidal Nanocrystals: S^{2-}, HS^{-}, Se^{2-}, HSe^{-}, Te^{2-}, HTe^{-}, TeS_3^{2-}, OH^{-}, and NH_2^{-} as Surface Ligands. *J. Am. Chem. Soc.* **2011**, *133*, 10612−10620.
(28) Zhang, H.; Hu, B.; Sun, L.; Hovden, R.; Wise, F. W.; Muller, D. A.; Robinson, R. D. Surfactant Ligand Removal and Rational Fabrication of Inorganically Connected Quantum Dots. *Nano Lett.* **2011**, *11*, 5356−5361.
(29) Guyot-Sionnest, P. Electrical Transport in Colloidal Quantum Dot Films. *J. Phys. Chem. Lett.* **2012**, *3*, 1169−1175.
(30) Ip, A. H.; Thon, S. M.; Hoogland, S.; Voznyy, O.; Zhitomirsky, D.; Debnath, R.; Levina, L.; Rollny, L. R.; Carey, G. H.; Fischer, A.; et al. Hybrid Passivated Colloidal Quantum Dot Solids. *Nat. Nanotechnol.* **2012**, *7*, 577−582.
(31) Ning, Z.; Ren, Y.; Hoogland, S.; Voznyy, O.; Levina, L.; Stadler, P.; Lan, X.; Zhitomirsky, D.; Sargent, E. H. All-Inorganic Colloidal Quantum Dot Photovoltaics Employing Solution-Phase Halide Passivation. *Adv. Mater.* **2012**, *24*, 6295−6299.
(32) Debnath, R.; Tang, J.; Barkhouse, D. A.; Wang, X.; Pattantyus-Abraham, A. G.; Brzozowski, L.; Levina, L.; Sargent, E. H. Ambient-Processed Colloidal Quantum Dot Solar Cells via Individual Pre-Encapsulation of Nanoparticles. *J. Am. Chem. Soc.* **2010**, *132*, 5952−5953.
(33) (a) Moody, I. S.; Stonas, A. R.; Lonergan, M. C. PbS Nanocrystals Functionalized with a Short-Chain, Ionic, Dithiol Ligand. *J. Phys. Chem. C* **2008**, *112*, 19383−19389.
(34) Hyun, B.-R.; Chen, H.; Rey, D. A.; Wise, F. W.; Batt, C. A. Near-Infrared Fluorescence Imaging with Water-Soluble Lead Salt Quantum Dots. *J. Phys. Chem. B* **2007**, *111*, 5726−5730.
(35) Kovalenko, M. V.; Bodnarchuk, M. I.; Zaumseil, J.; Lee, J.-S.; Talapin, D. V. Expanding the Chemical Versatility of Colloidal Nanocrystals Capped with Molecular Metal Chalcogenide Ligands. *J. Am. Chem. Soc.* **2010**, *132*, 10085−10092.
(36) Loiudice, A.; Rizzo, A.; Grancini, G.; Belviso, M. R.; Corricelli, M.; Curri, M. L.; Striccoli, M.; Agostiano, A.; Cozzoli, P. D.; Petrozza, A.; et al. Flexible All-Inorganic Nanocrystal Solar Cell by Room-Temperature Processing. *Energy Environ. Sci.* **2013**, *6*, 1565−1572.
(37) Altamura, D.; Lassandro, R.; Vittoria, F. A.; De Caro, L.; Siliqi, D.; Ladisa, M.; Giannini, C. X-ray Microimaging Laboratory (XMI-LAB). *J. Appl. Crystallogr.* **2012**, *45*, 869−873.
(38) Moreels, I.; Fritzinger, B.; Martins, J. C.; Hens, Z. Surface Chemistry of Colloidal PbSe Nanocrystals. *J. Am. Chem. Soc.* **2008**, *130*, 15081−15086.
(39) Mayr, H.; Breugst, M.; Ofial, A. R. Farewell to the HSAB Treatment of Ambident Reactivity. *Angew. Chem., Int. Ed.* **2011**, *50*, 6470−6505.
(40) Danehy, J. P.; Parameswaran, K. N. Acidic Dissociation Constants of Thiols. *J. Chem. Eng. Data* **1968**, *13*, 386−389.
(41) Masui, M.; Sayo, H.; Tsuda, Y. Anodic Oxidation of Amines. Part I. Cyclic Voltammetry of Aliphatic Amines at a Stationary Glassy-Carbon Electrode. *J. Chem. Soc. B* **1968**, 973−976.
(42) Jasieniak, J.; Mulvaney, P. From Cd-Rich to Se-Rich − the Manipulation of CdSe Nanocrystal Surface Stoichiometry. *J. Am. Chem. Soc.* **2007**, *129*, 2841−2848.
(43) Giansante, C.; Mazzanti, A.; Baroncini, M.; Ceroni, P.; Venturi, M.; Klärner, F.-G.; Vögtle, F. Tweezering the Core of Dendrimers: Medium Effect on the Kinetic and Thermodynamic Properties. *J. Org. Chem.* **2009**, *74*, 7335−7343.
(44) Owen, J. S.; Park, J.; Trudeau, P.-E.; Alivisatos, A. P. Reaction Chemistry and Ligand Exchange at Cadmium−Selenide Nanocrystal Surfaces. *J. Am. Chem. Soc.* **2008**, *130*, 12279−12281.
(45) Parks, J. S.; Cistola, D. P.; Small, D. M.; Hamilton, J. A. Interactions of the Carboxyl Group of Oleic Acid with Bovine Serum Albumin: a ^{13}C NMR Study. *J. Biol. Chem.* **1983**, *258*, 9262−9.
(46) Moreels, I.; Lambert, K.; Smeets, D.; De Muynck, D.; Nollet, T.; Martins, J. C.; Vanhaecke, F.; Vantomme, A.; Delerue, C.; Allan, G.; et al. Size-Dependent Optical Properties of Colloidal PbS Quantum Dots. *ACS Nano* **2009**, *3*, 3023−3030.
(47) Shaw, R. A.; Woods, M. Preparation and Some Properties of Lead Thiolates. *J. Chem. Soc. A* **1971**, 1569−1571.
(48) Eichhöfer, A. Four New Lead(II) Thiolate Cluster Complexes − Unexpected Products of a Conventional Synthesis. *Eur. J. Inorg. Chem.* **2005**, *2005*, 1683−1688.
(49) Magyar, J. S.; Weng, T.-C.; Stern, C. M.; Dye, D. F.; Rous, B. W.; Payne, J. C.; Bridgewater, B. M.; Mijovilovich, A.; Parkin, G.; Zaleski, J. M.; et al. Reexamination of Lead(II) Coordination Preferences in Sulfur-Rich Sites: Implications for a Critical Mechanism of Lead Poisoning. *J. Am. Chem. Soc.* **2005**, *127*, 9495−9505.
(50) Frederick, M. T.; Amin, V. A.; Cass, L. C.; Weiss, E. A. A Molecule to Detect and Perturb the Confinement of Charge Carriers in Quantum Dots. *Nano Lett.* **2011**, *11*, 5455−5460.
(51) Oliver, T. A. A.; Zhang, Y.; Ashfold, M. N. R.; Bradforth, S. E. Linking Photochemistry in the Gas and Solution Phase: S−H Bond Fission in P-Methylthiophenol Following UV Photoexcitation. *Faraday Discusss* **2011**, *150*, 439−458.
(52) Jasieniak, J.; Califano, M.; Watkins, S. E. Size-Dependent Valence and Conduction Band-Edge Energies of Semiconductor Nanocrystals. *ACS Nano* **2011**, *5*, 5888−5902.
(53) Yaacobi-Gross, N.; Soreni-Harari, M.; Zimin, M.; Kababya, S.; Schmidt, A.; Tessler, N. Molecular Control of Quantum-Dot Internal Electric Field and its Application to CdSe-Based Solar Cells. *Nat. Mater.* **2011**, *10*, 974−979.
(54) Hughes, B. K.; Ruddy, D. A.; Blackburn, J. L.; Smith, D. K.; Bergren, M. R.; Nozik, A. J.; Johnson, J. C.; Beard, M. C. Control of PbSe Quantum Dot Surface Chemistry and Photophysics Using an Alkylselenide Ligand. *ACS Nano* **2012**, *6*, 5498−5506.
(55) Wen, G. W.; Lin, J. Y.; Jiang, H. X.; Chen, Z. Quantum-Confined Stark Effects in Semiconductor Quantum Dots. *Phys. Rev. B* **1995**, *52*, 5913−5922.
(56) Wolcott, A.; Doyeux, V.; Nelson, C. A.; Gearba, R.; Lei, K. W.; Yager, K. G.; Dolocan, A. D.; Williams, K.; Nguyen, D.; Zhu, X. Y. Anomalously Large Polarization Effect Responsible for Excitonic Red Shifts in PbSe Quantum Dot Solids. *J. Phys. Chem. Lett.* **2011**, *2*, 795−800.
(57) Aoki, M.; Kamada, T.; Sasaki, K.; Masuda, S.; Morikawa, Y. Chemisorption-Induced Gap States at Organic−Metal Interfaces: Benzenethiol and Benzeneselenol on Metal Surfaces. *Phys. Chem. Chem. Phys.* **2012**, *14*, 4101−4108.
(58) Evers, W. H.; Nijs, B. D.; Filion, L.; Castillo, S.; Dijkstra, M.; Vanmaekelbergh, D. Entropy-Driven Formation of Binary Semiconductor-Nanocrystal Superlattices. *Nano Lett.* **2010**, *10*, 4235−4241.
(59) Choi, J. J.; Bealing, C. R.; Bian, K.; Hughes, K. J.; Zhang, W.; Smilgies, D.-M.; Hennig, R. G.; Engstrom, J. R.; Hanrath, T. Controlling Nanocrystal Superlattice Symmetry and Shape-Anisotropic Interactions through Variable Ligand Surface Coverage. *J. Am. Chem. Soc.* **2011**, *133*, 3131−3138.
(60) Bian, K.; Choi, J. J.; Kaushik, A.; Clancy, P.; Smilgies, D.-M.; Hanrath, T. Shape-Anisotropy Driven Symmetry Transformations in Nanocrystal Superlattice Polymorphs. *ACS Nano* **2011**, *5*, 2815−2823.
(61) Nagaoka, Y.; Chen, O.; Wang, Z.; Cao, Y. C. Structural Control of Nanocrystal Superlattices Using Organic Guest Molecules. *J. Am. Chem. Soc.* **2012**, *134*, 2868−2871.
(62) Romero, H. E.; Drndic, M. Coulomb Blockade and Hopping Conduction in PbSe Quantum Dots. *Phys. Rev. Lett.* **2005**, *95*, 156801.
(63) Jeong, K. S.; Tang, J.; Liu, H.; Kim, J.; Schaefer, A. W.; Kemp, K.; Levina, L.; Wang, X.; Hoogland, S.; Debnath, R.; et al. Enhanced Mobility-Lifetime Products in PbS Colloidal Quantum Dot Photovoltaics. *ACS Nano* **2012**, *6*, 89−99.
(64) Osedach, T. P.; Zhao, N.; Andrew, T. L.; Brown, P. R.; Wanger, D. D.; Strasfeld, D. B.; Chang, L.-Y.; Bawendi, M. G.; Bulović, V. Bias-

Stress Effect in 1,2-Ethanedithiol-Treated PbS Quantum Dot Field-Effect Transistors. *ACS Nano* **2012**, *6*, 3121−3127.
(65) Klem, E. J. D.; Shukla, H.; Hinds, S.; MacNeil, D. D.; Levina, L.; Sargent, E. H. Impact of Dithiol Treatment and Air Annealing on the Conductivity, Mobility, and Hole Density in PbS Colloidal Quantum Dot Solids. *Appl. Phys. Lett.* **2008**, *92*, 212105.
(66) Kang, M. S.; Sahu, A.; Norris, D. J.; Frisbie, C. D. Size- and Temperature-Dependent Charge Transport in PbSe Nanocrystal Thin Films. *Nano Lett.* **2011**, *11*, 3887−3892.
(67) Nagpal, P.; Klimov, V. I. Role of Mid-Gap States in Charge Transport and Photoconductivity in Semiconductor Nanocrystal Films. *Nat. Commun.* **2011**, *2*, 486.
(68) Voznyy, O.; Zhitomirsky, D.; Stadler, P.; Ning, Z.; Hoogland, S.; Sargent, E. H. A Charge-Orbital Balance Picture of Doping in Colloidal Quantum Dot Solids. *ACS Nano* **2012**, *6*, 8448−8455.
(69) Barkhouse, D. A. R.; Pattantyus-Abraham, A. G.; Levina, L.; Sargent, E. H. Thiols Passivate Recombination Centers in Colloidal Quantum Dots Leading to Enhanced Photovoltaic Device Efficiency. *ACS Nano* **2008**, *2*, 2356−2362.
(70) Gao, J.; Perkins, C. L.; Luther, J. M.; Hanna, M. C.; Chen, H.-Y.; Semonin, O. E.; Nozik, A. J.; Ellingson, R. J.; Beard, M. C. n-Type Transition Metal Oxide as a Hole Extraction Layer in PbS Quantum Dot Solar Cells. *Nano Lett.* **2011**, *11*, 3263−3266.
(71) Leschkies, K. S.; Beatty, T. J.; Kang, M. S.; Norris, D. J.; Aydil, E. S. Solar Cells Based on Junctions between Colloidal PbSe Nanocrystals and Thin ZnO Films. *ACS Nano* **2009**, *3*, 3638−3648.
(72) Hyun, B.-R.; Zhong, Y.-W.; Bartnik, A. C.; Sun, L.; Abruña, H. D.; Wise,, F. W.; Goodreau,, J. D.; Matthews, J. R.; Leslie, T. M.; Borrelli, N. F. Electron Injection from Colloidal PbS Quantum Dots into Titanium Dioxide Nanoparticles. *ACS Nano* **2008**, *2*, 2206−2212.
(73) Gao, J.; Jeong, S.; Lin, F.; Erslev, P. T.; Semonin, O. E.; Luther, J. M.; Beard, M. C. Improvement in Carrier Transport Properties by Mild Thermal Annealing of PbS Quantum Dot Solar Cells. *Appl. Phys. Lett.* **2013**, *102*, 043506.
(74) Bouclé, J.; Chyla, S.; Shaffer, M. S. P.; Durrant, J. R.; Bradley, D. D. C.; Nelson, J. Hybrid Solar Cells from a Blend of Poly(3-hexylthiophene) and Ligand-Capped TiO_2 Nanorods. *Adv. Funct. Mater.* **2008**, *18*, 622−633.